

# Graph-based Algorithm Unfolding for Energy-aware Power Allocation in Wireless Networks

Boning Li\*, Gunjan Verma†, and Santiago Segarra\*

\*Rice University, USA

†US Army DEVCOM Army Research Lab., USA

**Abstract**—We develop a novel graph-based trainable framework to maximize the weighted sum energy efficiency (WSEE) for power allocation in wireless communication networks. To address the non-convex nature of the problem, the proposed method consists of modular structures inspired by a classical iterative suboptimal approach and enhanced with learnable components. More precisely, we propose a deep unfolding of the successive concave approximation (SCA) method. In our unfolded SCA (USCA) framework, the originally preset parameters are now learnable via graph convolutional neural networks (GCNs) that directly exploit multi-user channel state information as the underlying graph adjacency matrix. We show the permutation equivariance of the proposed architecture, which promotes generalizability across different network topologies of varying size, density, and channel distribution. The USCA framework is trained through a stochastic gradient descent approach using a progressive training strategy. The unsupervised loss is carefully devised to feature the monotonic property of the objective under maximum power constraints. Comprehensive numerical results demonstrate outstanding performance and robustness of USCA over state-of-the-art benchmarks.

**Index Terms**—Wireless power allocation, multi-user multi-cell interference, weighted sum energy efficiency maximization, deep algorithm unfolding, graph convolutional neural networks.

## I. INTRODUCTION

Current and future wireless communication networks involve massive data transmission via their infrastructures while operating with limited resources [1–3]. Power is known to be a fundamental resource that requires efficient allocation to ensure the quality of wireless services [4]. In the meantime, the escalating size of modern wireless networks requires sustainable energy management to fulfill user demands with minimal power consumption [5]. To this end, the maximization of energy efficiency (EE) has been tackled from multiple perspectives including energy-efficient infrastructure design, network service deployment, and novel resource allocation strategies [6–8]. In particular, energy-efficient power allocation can help reduce greenhouse gas emissions and electromagnetic pollution [9], and it is also vital to reduce electricity budgets and prolong the battery life of mobile devices [10]. Our work

Research was sponsored by the Army Research Office and was accomplished under Cooperative Agreement Number W911NF-19-2-0269. B. Li was partially supported by the Ken Kennedy Institute 2020/21 Ken Kennedy-Cray Graduate Fellowship. The views and conclusions contained in this document are those of the authors and should not be interpreted as representing the official policies, either expressed or implied, of the Army Research Office or the U.S. Government. The U.S. Government is authorized to reproduce and distribute reprints for Government purposes notwithstanding any copyright notation herein.

E-mails: {boning.li, segarra}@rice.edu, gunjan.verma.civ@army.mil.

focuses on the energy-efficient allocation of transmit power in the uplink of a wireless interference network.

Mathematically, optimal power allocation takes the form of maximizing a system-level EE performance function subject to constraints on resource budgets. Despite the widespread use of traditional convex optimization in wireless communications [11–13], this theory is incapable of directly handling the problem at hand due to the nonconvex nature of EE metrics. Indeed, EE-oriented problems in interference-limited networks are typically NP-hard [14–16]. Although monotonic programming has been employed to reduce the computational time of branch-and-bound (BB) procedures [17, 18], the performance of such globally optimal methods scales poorly with the size of the network. Hence, several suboptimal methods based on optimization theory have been developed to obtain approximate power policies while promoting scalability. These classical methods can be broadly categorized into those based on interference cancellation [19], matching theory [20, 21], Lagrangian dual decomposition [22, 23], and successive convex (or concave) approximation (SCA) [18, 24–29]. Our special interest lies in the last of these classical approaches due to its popular adoption and guaranteed convergence. SCA has proven state-of-the-art performance in the maximization of some EE metrics such as the system global EE (GEE) [24, 25, 30] and the minimum of individual EE (MEE) [29, 31]. However, for metrics involving the weighted sum or product of node-wise EE there is a notable gap in performance between SCA solutions and global optima even with only seven users [17]. In addition, the time-varying channel characteristics pose a harsher requirement on computational efficiency as the allocation needs to be faster than the channel coherence time. In this context, the nested iterative nature of SCA can preclude its practical implementation. We seek to overcome these identified challenges by enhancing SCA with data-driven machine learning elements.

Deep neural networks (DNNs) have shown promising success in wireless power allocation and other communication problems [32–47]. Most of these approaches are model-free, meaning that they parameterize some function of interest with established multi-purpose architectures such as multi-layer perceptrons (MLPs) [32–34], convolutional neural networks (CNNs) [35, 36], recurrent neural networks [37], and graph neural networks (GNNs) [38, 40]. Hence, these approaches rely on the approximation capability of DNNs [48] to mimic the optimal solutions of classical optimization techniques based on solved examples. On the downside, these deep models do not tend to generalize well to unseen scenarios such

as shifts in channel distributions, varying network sizes, or user mobility. Moreover, obtaining a large set of labeled data, or optimal solutions in our case, as are needed to train DNNs in a supervised manner, may be infeasible for computationally intractable problems.

Our proposed solution combines classical (model-based) and learning-based (model-free) methodologies. The proposed approach is learning-based in the sense that it leverages stochastic gradient descent (SGD) to learn GNN parameters from simulated channel data. GNNs are able to exploit topological patterns of interference between users to locally process instantaneous channel state information (CSI). At the same time, our method is model-based since it takes advantage of the classical SCA algorithm by informing a stacked neural network architecture that imitates the iterative structure of SCA. Our goal is to achieve higher performance and faster computation than classical methods by combining the strengths of expert knowledge and statistical learning. Motivated by this, we adapt the paradigm of algorithm unfolding [49] to accomplish this synergistic combination.

**Related work.** The application of deep learning to wireless power allocation is an active area of research [32–45]. However, only a limited subset of these works utilize graph-based learning methods [38, 40, 43] or algorithm unfolding [41, 43–45]. The only prior work within power allocation that lives at the intersection (like our proposed approach) is [43, 50], which unfolds the iterative weighted minimum mean squared error (WMMSE) method for sum-rate maximization. Nonetheless, sum-rate is a different and theoretically simpler objective than the weighted sum EE (WSEE) here considered.

On a broader note, algorithm unfolding was first developed as a fast approximation of an iterative sparse coding algorithm [51]. Later on, many other iterative algorithms were unfolded, extending this scheme to a wide range of applications including image super-resolution [52], multi-channel source separation [53], compressive sensing [54], graph signal denoising [55], and precoding design [56]. In this context, we propose the unfolded successive concave approximation (USCA) method. To the best of our knowledge, this is the first graph-based deep unfolded architecture for the iterative SCA algorithm. By achieving performance and computational gains out of graph-based learning and algorithm unfolding respectively, USCA yields state-of-the-art performance in energy and computational efficiency for power allocation in wireless interference networks.

**Contribution.** The main contributions of this work are:

- i) We propose an unfolded version of SCA for energy-efficient power allocation in wireless interference networks, where traditional modules in the optimization algorithm are parameterized by learnable graph convolutional neural networks (GCNs). We also provide a thorough analysis on its computational complexity along with guidelines for distributed implementation.
- ii) In terms of theoretical analysis, Proposition 1 shows that the proposed method is permutation equivariant as long as the augmented learnable components satisfy this property.
- iii) Through numerical experimentation with wide-ranging

settings and configurations, we exemplify the advantageous performance of the proposed method compared with state-of-the-art alternatives, its generalizability to variations in network size and channel distribution, the potentials of transfer learning between different path-loss models, and the impact of imperfect supervision and training set size.

**Paper outline.** In Section II, we present the system model and formulate the power allocation problem as a constrained non-convex optimization problem. In Section III, we briefly introduce the classical SCA algorithm and provide a detailed description of the our proposed unfolded architecture. Theoretical analyses of permutation equivariance and computational complexity are presented in Sections III-B and III-C, respectively. In Section IV, we illustrate results of thorough numerical experimentation, demonstrating the superior performance of USCA in comparison with the original SCA and other benchmark methods, as well as its generalizability to changes in network settings and channel distributions. Finally, Section V closes this paper with conclusions and future directions.

**Notation.** Sets and maps are typeset in calligraphic letters  $\mathcal{A}$ . Alternative notations for sets  $\{a_i\}_{i=1}^n = \{a_1, \dots, a_n\}$  and vectors  $[a_i]_{i=1}^n = [a_1, \dots, a_n]$  are occasionally used for the purpose of clarification; when clear from context, we omit the size. Diagonal-related notations  $\text{diag}(\mathbf{A})$  and  $\text{diag}(\mathbf{a})$  denote a diagonal matrix storing diagonal elements of matrix  $\mathbf{A}$  or elements of vector  $\mathbf{a}$ , respectively.  $\mathbf{0}$  and  $\mathbf{1}$  denote all-zeros and all-ones vectors of appropriate size. Operations  $|\cdot|$ ,  $\|\cdot\|$ ,  $(\cdot)^\top$ ,  $(\cdot)^H$ ,  $\mathbb{E}(\cdot)$ , and  $[\cdot]_+$  denote absolute value,  $L^2$ -norm, transpose, conjugate transpose, expected value, and positive part, respectively. For conditional statements,  $\llbracket q \rrbracket = 1$  if  $q$  is true, 0 otherwise. Elementwise multiplication between two vectors (or two matrices) is denoted as  $\mathbf{a} \odot \mathbf{b}$ . The clipping operation  $\mathbf{x} := \mathbf{x}|_{[a,b]}$  denotes  $\mathbf{x}$  restricted to the set  $[a, b]$ . When applied to vectors, scalar functions or operators are applied in an elementwise manner. By default,  $\log$  is in base 2.

## II. SYSTEM MODEL & PROBLEM FORMULATION

We consider the uplink of a multi-cell interference network with  $L$  single-antenna users and  $M$  base stations (BSs). Each BS has  $n_R$  antennas. Let  $a(i)$  represent the BS serving user  $i$  for  $i = 1, \dots, L$ . Denoting the signal transmitted by  $i$  as  $x_i \in \mathbb{C}$ , the received signal  $\mathbf{y}_{a(i)} \in \mathbb{C}^{n_R}$  at BS  $a(i)$  is

$$\mathbf{y}_{a(i)} = \sum_{j=1}^L \mathbf{h}_{a(i),j} x_j + \mathbf{z}_{a(i)}, \quad (1)$$

where  $\mathbf{h}_{a(i),j} \in \mathbb{C}^{n_R}$  is the channel from  $j$  to  $a(i)$  and circularly-symmetric complex Gaussian noise  $\mathbf{z}_{a(i)} \sim \mathcal{N}_{\mathbb{C}}(0, \sigma_i^2)$  is added at receiver  $a(i)$  with power  $\sigma_i^2$ . Assuming matched filtering at the receiver and perfect channel estimation, the achievable data rate of the link from  $i$  to  $a(i)$  with bandwidth  $B$  can be derived as

$$R_i = B \log \left( 1 + \frac{\alpha_i p_i}{1 + \sum_{j \neq i} \beta_{i,j} p_j} \right), \quad (2)$$

where the CSI terms

$$\alpha_i = \frac{\|\mathbf{h}_{a(i),i}\|^2}{\sigma_i^2} \quad \text{and} \quad \beta_{i,j} = \frac{|\mathbf{h}_{a(i),i}^H \mathbf{h}_{a(i),j}|^2}{\sigma_i^2 \|\mathbf{h}_{a(i),i}\|^2}$$

are the channel gain over that link (which may be denoted by the user index for simplicity, i.e., link  $i$ ) and the multi-user interference from  $j$  to  $i$ , respectively. We define the multi-user CSI matrix  $\mathbf{H} \in \mathbb{R}^{L \times L}$  with channel gains as its diagonal entries and interference coefficients as off-diagonal entries, i.e.  $H_{i,j} = \mathbb{I}[j = i]\alpha_i + \mathbb{I}[j \neq i]\beta_{i,j}$ . Moreover, the average transmit power vector  $\mathbf{p} = [p_i]_{i=1}^L$  is subject to maximum power constraints  $\mathbf{P}_m = [P_{m,i}]_{i=1}^L$ . Notice that by introducing the CSI matrix  $\mathbf{H}$ , the system can now be interpreted as a directed graph with users as its nodes and  $\mathbf{H}$  as its adjacency matrix.

Furthermore, the link's achievable rate over its power consumption defines its energy efficiency (EE) in bits per joule, i.e.,

$$\text{EE}_i = \frac{B \log \left( 1 + \frac{H_{i,i} p_i}{1 + \sum_{j \neq i} H_{i,j} p_j} \right)}{\mu_i p_i + P_{c,i}}, \quad (3)$$

where  $\mu_i$  is the amplifier inefficiency in the transmitter  $i$ , and  $P_{c,i}$  is a constant portion of power consumed in  $i$  unrelated to the communication. With this notation in place, we formally state the maximum WSEE power allocation problem as follows

$$\begin{aligned} \max_{\mathbf{p}} \quad & \sum_{i=1}^L w_i \frac{\log \left( 1 + \frac{H_{i,i} p_i}{1 + \sum_{j \neq i} H_{i,j} p_j} \right)}{\mu_i p_i + P_{c,i}} \\ \text{s.t.} \quad & 0 \leq p_i \leq P_{m,i}, \quad i = 1, \dots, L. \end{aligned} \quad (\text{P1})$$

As mentioned in Section I, among various EE metrics, we consider the specific case of WSEE as the objective in (P1). Since WSEE depends on weighted efficiencies of individual users, certain users can be easily prioritized over others, thus fostering flexibility in heterogeneous networks. Nonetheless, it should be noted that the method proposed in Section III is general enough to apply to other EE metrics (such as GEE and MEE) and additional optimization constraints. For simplicity moving forward, in (P1) we consider uniform system constants  $\mu_i = \mu$  and  $P_{c,i} = P_c$  as well as uniform maximum power constraint  $P_{m,i} = P_m$  for all users  $i$ . However, our method can be applied to the non-uniform case seamlessly.

The objective in (P1) is a sum of fractions whose numerators are non-concave in general, making it an NP-hard problem [57]. Several approaches have been proposed to solve (P1), but either accuracy, tractability, or both have to be sacrificed [58]. In practice, a few approximate methods aim to solve for a local maximum of (P1). The performance of such traditional body of work depends on good initialization points, requiring the costly process of repeatedly solving a series of problems, each with a larger power constraint than its predecessor, until the actual target power constraint is reached. For this reason, we are motivated to develop an accurate, efficient, and scalable method that can generate near-optimal power allocations in near real-time.

### III. UNFOLDED SUCCESSIVE PSEUDO-CONCAVE APPROXIMATION (USCA) FRAMEWORK

Deep algorithm unfolding [49, 59, 60] is a collection of methods where iterative optimization algorithms are fused with tools from neural networks for greater computation efficiency and/or prediction accuracy. Zooming into the layers of unfolded neural networks, their architectures are usually inspired by existing algorithms specific to the task at hand. Since our system model, namely the multi-user wireless interference network, can be naturally modeled as a graph, we present our unfolded algorithm based on GNNs [61–63]. Indeed, we develop and evaluate a GCN-based framework [61] to unfold SCA, a first-order optimization algorithm for non-convex objectives. To the best of our knowledge, this is the first graph-based unfolded algorithm for *energy-efficient* power allocation.

In preparation for USCA, we first introduce the basics of SCA [18, 26]. Essentially, this classical algorithm handles the maximization of a non-concave function  $f$  by maximizing a sequence of (pseudo-)concave surrogate functions  $\{\tilde{f}_t(\mathbf{x}; \mathbf{x}^{(t)})\}_{t=0}^T$ . These surrogate functions must satisfy a series of assumptions stated in [26, Section III]. In the specific context of WSEE maximization, the objective in (P1) can be approximated through a series of concave functions (see [18, Section IV] for details)

$$\sum_{i=1}^L \widetilde{\text{EE}}_i(\mathbf{p}; \mathbf{p}^{(t)}) = \sum_{i=1}^L c_1 R_i(p_i, \mathbf{p}_{-i}^{(t)}) + c_2 p_i + c_3. \quad (4)$$

In (4),  $c_1$ ,  $c_2$  and  $c_3$  (whose explicit expression can be found in [18]) are constant coefficients given  $\mathbf{p}^{(t)}$ . User  $i$ 's data rate  $R_i(p_i, \mathbf{p}_{-i}^{(t)})$  [cf. (2)] is a function of its own power  $p_i$  alone, while other users transmit at fixed powers  $\mathbf{p}_{-i}^{(t)} = [p_j^{(t)}]_{j \neq i}^L$ . We observe that  $R_i(p_i, \mathbf{p}_{-i}^{(t)})$  is concave in  $p_i$ , from where the concavity of (4) with respect to  $p_i$  immediately follows. Approximating the objective of (P1) by (4), we obtain the following concave maximization problem

$$\begin{aligned} \max_{\mathbf{p}} \quad & \sum_{i=1}^L \widetilde{\text{EE}}_i(\mathbf{p}; \mathbf{p}^{(t)}) \\ \text{s.t.} \quad & 0 \leq p_i \leq P_m, \quad i = 1, \dots, L. \end{aligned} \quad (\text{P2})$$

We sequentially solve (P2) following the update policy on  $\mathbf{p}^{(t)}$  given by the line search

$$\mathbf{p}^{(t)} = \mathbf{p}^{(t-1)} + \gamma^{(t)} (\mathbb{B}\mathbf{p}^{(t)} - \mathbf{p}^{(t-1)}), \quad (5)$$

where  $\mathbb{B}\mathbf{p}^{(t)}$  is a global maximizer of (P2) at the  $t$ -th iteration. Using the Armijo rule [64], a scalar step size  $\gamma^{(t)}$  can be picked for a substantial update in the ascent direction, specific to the current iteration. Leveraging the convergence of the subproblems (P2), it has been shown in [26] that any limit point of  $\{\mathbf{p}^{(t)}\}$  is guaranteed to be a stationary point of (P1). Moreover, each of the subproblems (P2) can be solved in polynomial time using standard convex optimization methods such as interior-point methods or projected gradient descent [65, 66]. However, SCA requires nested iterations to solve (P2) and update (5) for convergence. Additionally, [18] has demonstrated that SCA

depends on sophisticated initializations<sup>1</sup> to land in good local optima, which makes its computation even more inefficient.

Intuitively, if we can find steeper ascent directions (i.e., a  $\mathbb{B}\mathbf{p}^{(t)}$  in (5) that need not be the exact global maximizer of the concave approximation but can be closer to the true non-approximated objective) and better step sizes (i.e., self-adaptive step sizes that can be different in every dimension) at each iteration, we can achieve higher performance with fewer iterations of these enhanced SCA blocks. With this motivation, we elucidate in the following section our proposed unfolded architecture USCA, where key functions of SCA are augmented by learnable neural networks.

### A. Proposed unfolding framework

**Architecture.** Our unfolded architecture (depicted in Fig. 1) is composed of multiple stacked layers where some key parameters, which used to be optimization-based, are now refined with learnable GCN-based subnetworks. More precisely, we propose to formulate the power allocation policy  $\mathbf{p} = \Phi(P_m, \mathbf{H}; \Theta)$  as a function of the CSI matrix  $\mathbf{H}$  and the power constraint  $P_m$  through a layered architecture  $\Phi$  with trainable weights  $\Theta = [\Theta_{\text{emb}}, \Theta_p^{(1)}, \Theta_s^{(1)}, \dots, \Theta_p^{(T)}, \Theta_s^{(T)}]$ .

To understand the USCA architecture in Fig. 1, first notice that it consists of  $T$  blocks, preceded by a single embedding block. The input to a generic block  $t + 1$  is  $\mathbf{Z}^{(t)} = [\mathbf{p}_{\text{emb}}^{(t)}, \mathbf{p}^{(t)}] \in \mathbb{R}^{L \times 2}$ , which consists of the horizontal concatenation of an embedding vector  $\mathbf{p}_{\text{emb}}^{(t)} \in \mathbb{R}^L$  and the current power allocation  $\mathbf{p}^{(t)} \in \mathbb{R}^L$  determined by the first  $t$  blocks. The power allocation output by USCA is  $\mathbf{p}^{(T)}$ , which can be directly read from the second column of  $\mathbf{Z}^{(T)}$ , the output of the  $T$ -th block. The input  $\mathbf{Z}^{(0)}$  to the first unfolded block is given by the embedding block in Fig. 1. More precisely,

$$\mathbf{Z}^{(0)} = [\mathbf{p}_{\text{emb}}^{(0)}, \mathbf{p}^{(0)}] = [\Psi_{\text{emb}}(\mathbf{1}, \mathbf{H}; \Theta_{\text{emb}}), P_m \mathbf{1}], \quad (6)$$

where  $\mathbf{p}^{(0)}$  is set as a constant vector of value  $P_m$  and  $\mathbf{p}_{\text{emb}}^{(0)}$  is obtained as the output of the GCN  $\Psi_{\text{emb}}$ .

For completeness, we provide here the structure of a generic  $Q$ -layer GCN  $\Psi$  with input  $\mathbf{Z}$  and trainable parameters  $\Theta$  acting on the CSI matrix  $\mathbf{H}$ . Denoting the input as  $\mathbf{X}^0 = \mathbf{Z}$ , then  $\mathbf{Z}' = \Psi(\mathbf{Z}, \mathbf{H}; \Theta) = \mathbf{X}^Q$ , where an intermediate  $q$ -th layer of the GCN is given by

$$\mathbf{X}^q = \sigma_q \left( \mathbf{D}^{-\frac{1}{2}} \mathbf{H} \mathbf{D}^{-\frac{1}{2}} \mathbf{X}^{q-1} \Theta^q \right). \quad (7)$$

In (7),  $\mathbf{D} = \text{diag}(\mathbf{H}\mathbf{1})$ ,  $\Theta^q \in \mathbb{R}^{d_{q-1} \times d_q}$  are the trainable parameters,  $d_{q-1}$  and  $d_q$  are the dimensions of the output features of layers  $q - 1$  and  $q$ , respectively, and  $\sigma_q(\cdot)$  is the activation function. The specifics of the number of layers  $Q$ , the hidden dimensions  $d_q$ , and the activations functions  $\sigma_q$  used in our experiments are further detailed in Section IV.

We are left to explain the inner workings of a generic unfolded block  $t$ , so that we can obtain  $\mathbf{Z}^{(t)}$  from  $\mathbf{Z}^{(t-1)}$

<sup>1</sup>When solving for  $\mathbf{p}_K$  with constraint  $P_{m_K}$ , a sequence of  $\{\mathbf{p}_0, \dots, \mathbf{p}_K\}$  are sequentially solved for with ascending power constraints from  $P_{m_0}$  through  $P_{m_K}$ . In each pass, the initial point for  $\mathbf{p}_k$  is set to the optimal solution obtained for  $\mathbf{p}_{k-1}$  (i.e., the optimal solution obtained for the previous smaller constraint).

(detailed in Fig. 1 for  $t = 1$ ). The first operation is given by the GCN  $\Psi_p$ , from which we obtain

$$\mathbb{B}\mathbf{Z}^{(t)} = [\mathbf{p}_{\text{emb}}^{(t)}, \mathbb{B}\mathbf{p}^{(t)}] = \Psi_p(\mathbf{Z}^{(t-1)}, \mathbf{H}; \Theta_p^{(t)}). \quad (8)$$

The first column  $\mathbf{p}_{\text{emb}}^{(t)}$  of the output in (8) updates the node embeddings and directly constitutes the first column of  $\mathbf{Z}^{(t)}$ . On the other hand, the second column  $\mathbb{B}\mathbf{p}^{(t)}$  of the output in (8) is used to update  $\mathbf{p}^{(t)}$  following the expression [cf. (5)]

$$\mathbf{p}^{(t)} = \left( \mathbf{p}^{(t-1)} + \gamma^{(t)} \odot (\mathbb{B}\mathbf{p}^{(t)} - \mathbf{p}^{(t-1)}) \right) \Big|_{[0, P_m]}. \quad (9)$$

There are several differences between (9) and its classical counterpart (5). First, in (9) we obtain  $\mathbb{B}\mathbf{p}^{(t)}$  as the output of a GCN  $\Psi_p$  compared to the more computationally complex procedure of solving (P2) in classical SCA. Second, the output of the update in (9) is clipped to the interval  $[0, P_m]$  to guarantee that  $\mathbf{p}^{(t)}$  is a feasible power allocation for any intermediate block  $t$ . Lastly, the step size  $\gamma^{(t)}$  in (9) is a vector (as opposed to a scalar in (5)) and is set via a GCN  $\Psi_s$  instead of the Armijo rule. More precisely, we have that

$$\gamma^{(t)} = \left( \Psi_s([\mathbf{Z}^{(t-1)}, \mathbb{B}\mathbf{p}^{(t)}], \mathbf{H}; \Theta_s^{(t)}) \right) \Big|_{[0, 1]}. \quad (10)$$

The step size expression in (10) is motivated by the classical line search in that it depends on both the previous  $\mathbf{p}^{(t-1)}$  (contained in  $\mathbf{Z}^{(t-1)}$ ) and the solution  $\mathbb{B}\mathbf{p}^{(t)}$  to the current approximation. Besides, (10) extends the classical Armijo rule to accommodate different step sizes for different nodes, instead of a common one for every node. In addition, the channel information is also taken into consideration in the step size computation. Intuitively, this additional flexibility can help in achieving faster convergence.

The entire framework is trained by minimizing a tailored loss function and following a sequential strategy, which we elaborate in the sequel.

**Loss function.** Given parameters  $\Theta$ , the allocated power from USCA for a channel-constraint instance is  $\mathbf{p} = \Phi(P_m, \mathbf{H}; \Theta)$ . By denoting the objective of (P1) as  $\text{WSEE}(\mathbf{p}, \mathbf{H})$ , where we have made explicit its dependence on the power allocation and the channel state, we define the unsupervised loss function

$$\mathcal{L}_u(\Theta) = -\mathbb{E}_{\mathbf{H} \sim \mathcal{H}} [\text{WSEE}(\Phi(P_m, \mathbf{H}; \Theta), \mathbf{H})], \quad (11)$$

where  $\mathcal{H}$  is a known channel distribution from which we draw samples of  $\mathbf{H}$ .

We augment this loss with two regularizers that allow us to incorporate additional domain knowledge to our learning procedure. The first regularizer leverages the fact that the WSEE objective in (P1) must be monotonically non-decreasing with respect to the maximum allowable power  $P_m$  in the constraints. The intuition is straightforward, larger values of  $P_m$  correspond to strictly larger feasible sets in (P1), which can never result in smaller objective values. Accordingly, we devise a regularizer for our USCA loss that penalizes deviation from this desired monotonic relation. More precisely, we set a small  $\Delta P > 0$  and for every  $P_m$  of interest we consider the output of our USCA model when perturbing the

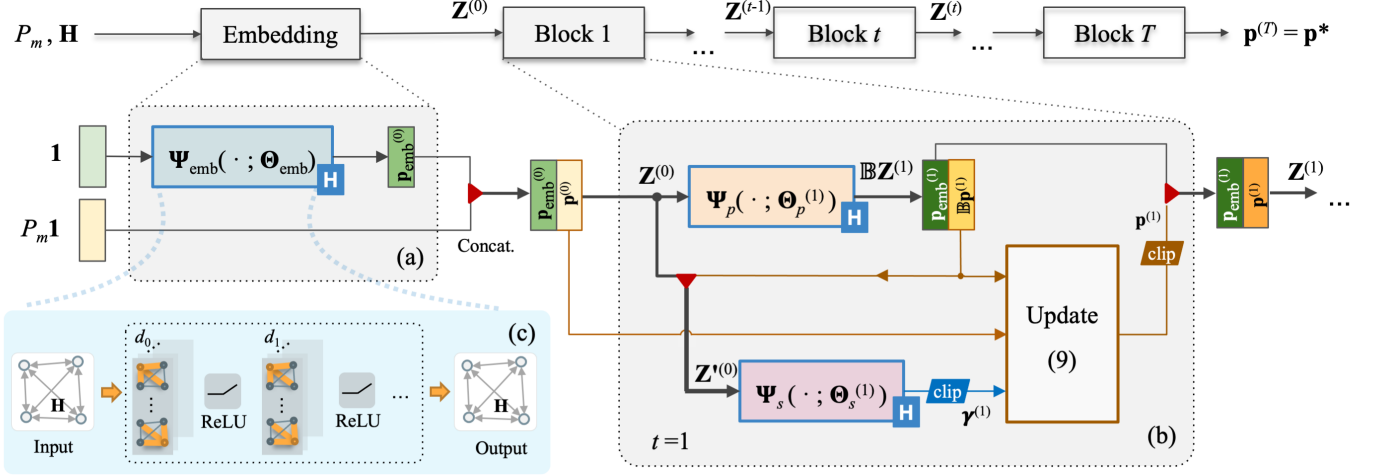


Fig. 1: Overall schematic view of our proposed USCA architecture for energy-efficient power allocation. (a) The embedding block. This block encodes channel information through a GCN  $\Psi_{\text{emb}}$ , whose output is concatenated with  $P_m \mathbf{1}$  to form the input to the first USCA block. (b) The USCA block. This block contains two GCNs ( $\Psi_p$  and  $\Psi_s$ ) that respectively mimic the classical operations in SCA of solving problem (P2) and finding the step size to update the power allocation. The outputs of these GCNs are combined following the update in (9), whose functional form is inspired by the classical counterpart. (c) The GCN. A schematic view of a generic GCN with feature dimensions being  $d_0, d_1, \dots$  and ReLU non-linearities. The three GCNs in our model ( $\Psi_{\text{emb}}$ ,  $\Psi_p$ , and  $\Psi_s$ ) employ this basic architecture.

maximum allowable power as  $p_- = \Phi(P_m - \Delta P, \mathbf{H}; \Theta)$ . (12), and (13)]

The monotonic regularization is then defined as

$$\mathcal{R}_m(\Theta) = \mathcal{R}_1(\Theta) + \lambda_s \mathcal{R}_2(\Theta), \quad (12)$$

where  $\mathcal{R}_1 = [\text{WSEE}(\mathbf{p}_-, \mathbf{H}) - \text{WSEE}(\mathbf{p}, \mathbf{H})]_+$  is a hinge loss that penalizes violations from monotonicity and  $\mathcal{R}_2$  is a self-supervisory Huber loss between original predictions and the auxiliary allocation for instances with positive  $\mathcal{R}_1$ , i.e.,  $\mathcal{R}_2(\Theta) = \llbracket \mathcal{R}_1 > 0 \rrbracket \phi(\bar{\mathbf{p}}, \bar{\mathbf{p}}_-)$ , where  $\phi$  is the classical Huber loss for robust regression [67]. The relative importance between  $\mathcal{R}_1$  and  $\mathcal{R}_2$  is given by the coefficient  $\lambda_s$  (default:  $1 \times 10^3$ ). Notice that  $\mathcal{R}_m(\Theta)$  is non-zero only when monotonicity is violated, thus avoiding the incorporation of an unnecessary regularizer when monotonicity is already satisfied.

As a second regularizer we consider a supervised loss whenever solved instances of (P1) are available. The supervision can then be expressed as

$$\mathcal{L}_s(\Theta) = \phi(\Phi(P_m, \mathbf{H}; \Theta), \mathbf{p}_{\text{opt}}), \quad (13)$$

where  $\phi$  is a Huber loss and  $\mathbf{p}_{\text{opt}}$  is a pre-specified optimal power allocation for channel  $\mathbf{H}$  and power constraint  $P_m$ . Nevertheless, it must be stressed that the training of USCA does not necessarily require supervision since we have the option of not incorporating the supervised loss in (13). In fact, global optimal allocations can be hard to acquire, as we emphasized in Section II. That being the case, we identify USCA as an unsupervised method since the access to optimal power allocations  $\mathbf{p}_{\text{opt}}$  is optional rather than essential.

To sum up, we propose the following overall loss function as the weighted sum of all the aforementioned terms [cf. (11),

$$\mathcal{L}(\Theta) = \mathcal{L}_u(\Theta) + \eta_m \mathcal{R}_m(\Theta) + \eta_s \mathcal{L}_s(\Theta), \quad (14)$$

where  $\eta_m$  and  $\eta_s$  (default: 0) are configured to balance the main loss with regularization and supervision, respectively. Leveraging the fact that  $\mathcal{L}(\Theta)$  in (14) is differentiable with respect to  $\Theta$ , we seek to minimize the loss via SGD. Additional details on the training strategy are provided next.

**Training strategy.** In order to stabilize training, especially for deeper USCA architectures (larger number of blocks  $T$ ), we use a progressive training strategy to enhance our end-to-end learning process. Similar strategies are widely used in the deep unfolding literature [68, 69]. In principle, the idea is to train the blocks one-by-one while decaying the learning rate by depth. More precisely, we first train the parameters of the  $t = 1$  block (in our case, the embedding block as well). We then freeze the trained parameters and train the next  $t = 2$  block. After this, we fine-tune all parameters within the trained blocks. Subsequently, all previous blocks are fixed and we proceed to add the  $t = 3$  block into the training procedure, and so on. As training progresses to deeper blocks, learning rates of shallower blocks are exponentially decayed to prevent their parameters from varying too wildly.

The proposed training method should be interpreted differently from classical layered neural networks where different layers tend to learn distinct functionalities [70]. On the contrary, all USCA blocks are producing the same type of output in essence – all provide a feasible power allocation vector. In this sense, if the previous  $t - 1$  blocks have been well trained and their output  $\mathbf{p}^{(t-1)}$  (which is also the input to the  $t$ -th block) is close-to-optimal, training the  $(t + 1)$ -th block

would become much easier – something not too far away from an identity map. Thus, these blocks share functional similarity and can indeed benefit from progressive training. Unless otherwise stated, all unfolding models reported in Section IV are trained using the above strategy.

### B. Permutation equivariance

As one of the most popular implementations of graph-based neural networks, GCNs are simple and concise, making them a suitable choice for our  $\Psi$  functions in USCA. GCNs are composed of graph filters which are similar to convolutional filters in classical CNNs [71]. Those graph filters learn to perform appropriate local aggregations through trainable parameters. Importantly, selecting GCNs as our functions  $\Psi$  confers our USCA framework with *permutation equivariance*, as we explain next. Let us begin by formally introducing this property. Consider the set  $\mathcal{F}$  of functions  $f : \mathbb{R}^{N \times N} \rightarrow \mathbb{R}^{N \times M}$ , the set  $\mathcal{G}$  of functions  $g : \mathbb{R}^{N \times M'} \times \mathbb{R}^{N \times N} \rightarrow \mathbb{R}^{N \times M}$ , and a generic permutation matrix  $\Pi \in \{0, 1\}^{N \times N}$ .

**Definition 1.** A function  $f \in \mathcal{F}$  is *permutation equivariant* if  $f(\Pi \Pi \Pi^\top) = \Pi f(\Pi)$  for all matrices  $\Pi$  and all permutations  $\Pi$ . Similarly, a function  $g \in \mathcal{G}$  is *permutation equivariant* if  $g(\Pi \mathbf{Z}, \Pi \Pi \Pi^\top) = \Pi g(\mathbf{Z}, \Pi)$  for all matrices  $\mathbf{Z}, \Pi$  and all permutations  $\Pi$ .

With permutation equivariance, simply changing the ordering or labeling of nodes in a network at the input does not change the output values in each individual node. Rather, the outputs are reordered or relabeled in the same manner as the input. We emphasize this property because it is particularly germane to our application where node (or user) indexing is arbitrary and, thus, should not cause any bias to power allocation results. Notice that the entire USCA framework can be interpreted as belonging to  $\mathcal{F}$  for  $N = L$  and  $M = 1$  since it maps  $\mathbf{H}$  to  $\mathbf{p}$ . By contrast, individual functions  $\Psi$  within USCA admit as inputs  $\mathbf{H}$  and a series of node features, thus belonging to  $\mathcal{G}$ . Indeed, as building bricks of USCA, the functions  $\Psi$  determine whether or not the whole framework is permutation equivariant, as we show next.

**Proposition 1.** If all basic subnetworks  $\Psi_{\text{emb}}$ ,  $\Psi_p$ , and  $\Psi_s$  are permutation equivariant, then the USCA framework  $\Phi$  is also permutation equivariant.

*Proof.* We want to show that  $\Phi(P_m, \Pi \Pi \Pi^\top; \Theta) = \Pi \Phi(P_m, \Pi; \Theta)$  for every  $\Pi$  and  $\Theta$ , where the parameters  $\Theta$  and the maximum power  $P_m$  are fixed. This can be proved by showing that the embedding block and a generic USCA block  $t$  in Fig. 1 are permutation equivariant, and by noting that composing a series of these operations preserves permutation equivariance.

That the embedding block is permutation equivariant directly follows from  $\Psi_{\text{emb}}$  satisfying this property combined with the fact that the second column of the block's output  $\mathbf{p}^{(0)}$  is a constant vector  $P_m \mathbf{1}$ . Thus,  $\mathbf{p}^{(0)} = \Pi \mathbf{p}^{(0)}$  for any permutation matrix  $\Pi$ .

For a generic USCA block  $t$ , we want to show that when the input to the block is  $\tilde{\mathbf{Z}}^{(t-1)} := \Pi \mathbf{Z}^{(t-1)}$  and we consider

the channel matrix  $\tilde{\mathbf{H}} := \Pi \mathbf{H} \Pi^\top$ , the output of the block is given by  $\tilde{\mathbf{Z}}^{(t)} = \Pi \mathbf{Z}^{(t)}$ . Notice that we use  $(\cdot)$  to denote intermediate variables within the USCA block when the input and the channel matrix have been permuted. From (8) and permutation equivariance of  $\Psi_p$ , it follows that  $\tilde{\mathbf{p}}_{\text{emb}}^{(t)} = \Pi \mathbf{p}_{\text{emb}}^{(t)}$  and  $\tilde{\mathbf{B}} \tilde{\mathbf{p}}^{(t)} = \Pi \mathbf{B} \mathbf{p}^{(t)}$ . Moreover, combining this last equality with (10) and recalling that  $\Psi_s$  is assumed to be permutation equivariant we have that

$$\begin{aligned} \tilde{\gamma}^{(t)} &= \left( \Psi_s([\tilde{\mathbf{Z}}^{(t-1)}, \tilde{\mathbf{B}} \tilde{\mathbf{p}}^{(t)}], \tilde{\mathbf{H}}; \Theta_s^{(t)}) \right) \Big|_{[0,1]} \\ &= \left( \Psi_s(\Pi[\mathbf{Z}^{(t-1)}, \mathbf{B} \mathbf{p}^{(t)}], \Pi \mathbf{H} \Pi^\top; \Theta_s^{(t)}) \right) \Big|_{[0,1]} = \Pi \gamma^{(t)}. \end{aligned}$$

Finally, inputting these expressions into the update (9) we get that

$$\begin{aligned} \tilde{\mathbf{p}}^{(t)} &= \left( \tilde{\mathbf{p}}^{(t-1)} + \tilde{\gamma}^{(t)} \odot (\mathbf{B} \tilde{\mathbf{p}}^{(t)} - \tilde{\mathbf{p}}^{(t-1)}) \right) \Big|_{[0, P_m]} \\ &= \left( \Pi \mathbf{p}^{(t-1)} + \Pi \gamma^{(t)} \odot (\Pi \mathbf{B} \mathbf{p}^{(t)} - \Pi \mathbf{p}^{(t-1)}) \right) \Big|_{[0, P_m]} = \Pi \mathbf{p}^{(t)}, \end{aligned}$$

where the last equation follows from the fact that all the operations in the update are elementwise. Hence, we have established that the output of a generic USCA block is given by  $\tilde{\mathbf{Z}}^{(t)} = [\tilde{\mathbf{p}}_{\text{emb}}^{(t)}, \tilde{\mathbf{p}}^{(t)}] = [\Pi \mathbf{p}_{\text{emb}}^{(t)}, \Pi \mathbf{p}^{(t)}] = \Pi \mathbf{Z}^{(t)}$ , as wanted.  $\square$

Combining Proposition 1 with the well-established fact that GCNs are permutation equivariant [72], we can conclude that *the proposed USCA framework is permutation equivariant*.

Conveniently, the modular structure of USCA depicted in Fig. 1 enables the practitioner to choose alternative architectures for the subnetworks  $\Psi$ . The loss function can also be seamlessly reformulated if different objective functions or constraints are of more interest. In Section IV, the performance of other candidate  $\Psi$  architectures is introduced and compared. In this setting, Proposition 1 guarantees that, as long as the  $\Psi$  functions are permutation equivariant, the USCA framework will also enjoy this favorable property.

**Remark 1** (Flexibility to varying number of users). Different from many neural network applications with fixed input and output dimensions, communication systems are a more challenging scenario as the number of users in the system can vary over time. This requires USCA to be able to output a power allocation strategy for a number of users  $L'$  different from the  $L$  users with which it was trained. This distinguishing capability is achieved by relying on graph neural networks and is numerically showcased in Section IV-B.

### C. Computational complexity

In the broad field of non-convex optimization, a fundamental benefit of learning-based methods over traditional model-based algorithms lies in the reduced computational complexity when presented with a new sample. In contrast to model-based methods which have to run from scratch whenever an unseen sample is given, learning-based methods present a fundamental trade-off where expensive computations for

training (e.g., computing gradients and back propagation, and constructing the dataset if required) can be performed *offline*, leaving only a few simple computations to be performed *online* regularly (e.g., affine transformation, scalar multiplication, and pointwise nonlinearity). Retraining or fine-tuning may be recommended when the real input distribution shifts far away from the trained one, but only sporadically and, typically, with fewer data.

In terms of offline complexity, it should be recalled that USCA can be trained in the absence of solved instances of the power allocation problem. Hence, effectively circumventing the need to solve several NP-hard problems for training. Nevertheless, since we are interested in the feasibility of real-time implementation, we focus our analysis on the online computational complexity.

To better understand the online complexity of USCA, let us focus on a generic unfolding block in Fig. 1 since the embedding block has fewer computations and equivalent asymptotic complexity. From (7) it follows that a generic USCA block involves  $\sum_{q=1}^Q (L^2 d_{q-1} + d_{q-1} L d_q)$  real multiplications (additions neglected) and  $\sum_{q=1}^{Q+1} L d_q$  non-linear activations to compute  $\mathbb{B}\mathbf{Z}^{(t)}$  as the output of  $\Psi_p$ . Similarly, computations in the other GCN subnetwork  $\Psi_s$  can be broken down as above. Together with clipping operations and updating rule (9) – each requiring  $\mathcal{O}(L)$  complexity –, the overall time complexity of USCA with respect to the number of users is  $\mathcal{O}(L^2)$ . On the other hand, classical SCA requires several solutions of the convex optimization problem (P2) each of them with polynomial complexity (whose specific form will depend on the algorithm chosen) plus determining the step size  $\gamma(t)$  with linear time complexity. As illustrated in Section IV-A, it is not only the case that one USCA block entails less computations than solving one instance of (P2) but also the number of USCA blocks  $T$  needed for good performance is typically less than the iterations needed in classical SCA. On top of that, the progressive training strategy can further minimize block numbers in the final USCA framework by simply cutting off at the block where EE metrics flatten out.

Lastly, USCA is amenable to a distributed deployment, which can bring about extra time efficiency in practice. This feature is inherited from the graph neural networks  $\Psi$  building USCA, which can be naturally implemented in a distributed manner [71]. However, it should be noted that training should be performed in a centralized manner and, once training is complete, the whole set of USCA parameters  $\Theta$  must be broadcasted to every user. Although the offline phase cannot be distributed, a distributed online phase can facilitate scalability of the proposed solution to large communication systems.

#### IV. NUMERICAL EVALUATION

We demonstrate and validate the performance of USCA through extensive numerical experiments in various settings<sup>2</sup>. Section IV-A compares USCA with other candidate approaches, where training and test data are drawn from the

same channel distribution. We then test the generalizability of the proposed method to changes in the network density and size (Section IV-B) and to changes in the channel distribution (Section IV-C). Finally, in Section IV-D we analyze up to what extent labeled data can aid the learning process.

Our experimental setup follows the one considered in [18]. More precisely, we consider  $M$   $n_R$ -antenna BSs located at the center of  $M$  ( $M = m^2$  for some  $m \in \mathbb{Z}$ ) adjacent non-overlapping square cells of side 1 km forming a squared overall coverage area of side  $m$  km. In each BS, the received noise power  $\sigma^2 = FN_0B$  is defined with noise figure  $F = 3$  dB, noise density  $N_0 = -174$  dBm/Hz, and bandwidth  $B = 180$  kHz. Within the overall coverage area,  $L$  single-antenna users, all with  $P_c = 1$  W and  $\mu = 4$ , are placed uniformly at random static locations. We primarily consider  $M = 4$ ,  $L = 8$ ,  $n_R = 1$ , as well as the wideband spatial (WBS) path loss (PL) propagation model [73] with Gaussian fast fading for the generation of training data. Test data may be configured differently and this will be explicitly discussed as we go into details about configurations of each experiment. Unless otherwise specified, the training dataset includes 1000 random channel realizations equally split into two subsets, one for training and the other for validation in a 2-fold cross validation manner. Coupled with 51 maximum power constraints which are integers in decibel units ranging from  $-40$  to  $10$  dBW (which are converted to Watts when input to USCA), it gives us 51,000 channel-constraint samples in total. The test set has the same number of independent channel realizations and identical power constraints as the training set.

Our proposed USCA method solves (P1) through 8 sequentially connected blocks (1 embedding block and  $T = 7$  unfolding blocks). The subnetworks  $\Psi$  are given by 5-layer GCNs with hidden dimensions equal to  $\{8, 32, 32, 16, 8\}$ , respectively, each followed by ReLU activation. ADAM optimizer with  $\ell_2$  coefficient of  $1 \times 10^{-6}$  is employed.

Progressive training works as follows. For  $\tau \in \{1, \dots, T\}$ , 1) fix all parameters in the previous blocks (from the first one<sup>3</sup> through  $t = \tau - 1$ ) with initial leaning rate  $l_0 = 1 \times 10^{-3}$ ; 2) unfreeze all parameters and train  $t \in \{1, \dots, \tau\}$  blocks respectively with block-wise learning rates, namely  $l_t = d^{\tau-t} d_l l_0$  for the  $t$ -th block, wherein  $d = 0.6$  and  $d_l = 0.4$  are empirical decay rates. Both steps are repeatedly performed with a maximum of 1000 epochs with early stopping to avoid over-training. Termination is triggered by over  $n_1 = 50$  (for step-1) or  $n_2 = 100$  (for step-2) epochs of unchanged best WSEE performance on the validation set. At the beginning of each epoch, all 25,500 training samples are randomly shuffled and split into 50 non-overlapping mini-batches of size 510.

##### A. Performance comparison

To begin with, we present a thorough comparison between the performance of our proposed GCN-based USCA algorithm (GCN-USCA, or simply USCA) with that of the original SCA algorithm and several other established baselines. The candidate methods are listed and explained as follows.

<sup>2</sup>The implementation of our method is available at [https://github.com/bl166/usca\\_power\\_control](https://github.com/bl166/usca_power_control). All experiments were conducted using an NVIDIA GeForce GTX 1080 Ti Graphics Card.

<sup>3</sup>Here, for the simplicity of notation, we treat the embedding block as within the  $t = 1$  block as a whole.

- 1) **SCA** serves as the benchmark method because it is the original algorithm inspiring this work and is also a commonly used state-of-the-art suboptimal algorithm to address this problem. We set a sufficiently large enough upper limit of 500 inner solver iterations, i.e., iterations in solving a single instance of (P2) (via projected gradient descent with adaptive learning rate [74]); and 700 outer iterations of successive approximation, i.e., updates as described in (5).
- 2) **Tr-SCA**, or the truncated SCA, forms a lower bound of achievable WSEE of SCA with as many iterations as USCA. We fix the number of inner and outer iterations of Tr-SCA to 5 and 7, respectively, to match the USCA unfolding (5 layers in  $\Psi$  and  $T = 7$  unfolding blocks). It is also based on the fine-tuned power initialization as mentioned in footnote 1 (Page 4).
- 3) **MLP-USCA** is implemented as an MLP-based USCA framework, simply by replacing GCNs  $\Psi$  with MLPs. The inputs to each block are concatenations of flattened logarithmic values of  $\mathbf{H}$  and intermediate features  $\mathbf{Z}^{(t)}$ . This is to show the versatility of graph-based learning principles in wireless communication networks.
- 4) **GCN** without unfolding is also included to highlight the effectiveness brought about by the SCA-inspired architecture. This is a plain GCN with  $\mathbf{H}$  as adjacency matrix, as well as  $P_m$  as input signal and  $p_i$  as output signal at node  $i$ . To compensate for the capacity of learnable parameters, it is implemented as a 5-layer GCN with hidden dimensions equal to  $\{56, 224, 224, 112, 56\}$  and trained in an end-to-end manner with  $\eta_m = 0.25$ ;
- 5) **Max-Pow** designates to all users the maximal possible transmit power, i.e.,  $p_i = P_m$  for all  $i = 1, \dots, L$ . This naive strategy works well for small  $P_m$  values before interference starts to dominate EE metrics.
- 6) **Opt** is the globally optimal solution given by the BB procedure using monotonic optimization [18]. Due to its high complexity for large network sizes, similar to [18], we provide results only for the 6-user network.

We perform these comparisons on the basis of the WBS model and report the results in Fig. 2. In a nutshell, the results show that the proposed GCN-USCA outperforms all other methods. The average WSEE against  $P_m$  values over 1000 test channel realizations achieved by candidate methods are displayed in Fig. 2a. From the figure it follows that GCN-USCA yields the largest WSEE values for every choice of the power constraint bound  $P_m$ . In particular, GCN-USCA largely improves with respect to the SCA baseline, underscoring the value of the proposed unfolded framework. Moreover, the fact that GCN-USCA works better than both MLP-USCA and GCN indicates that it is the combination of the unfolding and the use of graph neural networks what provides the performance boost attained by our proposed method.

In Fig. 2b we further compare GCN-USCA with the classical SCA and its truncated version. Notice that due to randomness in channel generation, the achievable utility metric of each channel realization can be notably different even with fixed power constraint. This is illustrated in the figure, where we present a histogram of the average WSEE value over

all power constraints for a channel realization. According to these empirical distributions, Tr-SCA matches the performance of SCA for most channel realizations (even though being surpassed in a few cases), but they both are outperformed by GCN-USCA. To be exact, GCN-USCA, SCA, and Tr-SCA respectively achieve average WSEE of 6.766, 6.148, and 6.131 bit/J. Compared with the full SCA, the performance degradation in Tr-SCA is not surprising because of the limited number of iterations allowed. Tr-SCA pays a price in allocation accuracy for lower computational cost. To be specific, allocating power under the 51 constraint values for one channel instance costs on average 0.32 sec. for Tr-SCA but 5.44 sec. for SCA. GCN-USCA surpasses this gap by learning more intelligent approximations and update steps to converge faster to the optimal within as many iterations as Tr-SCA. It takes only 0.094 sec. to finish one pass of the aforementioned task. Additionally, GCN-USCA can perform allocation in a one-shot manner, i.e., it treats individual channel-constraint samples as independent instances. This is fundamentally different from and favored over the classical benchmarks where allocation under higher constraint values needs to be calibrated by sufficiently small constraint values (e.g.,  $P_m \ll -10$  dBW in Fig. 2a) to ensure good performance.

When comparing GCN-USCA with learning-based methods, it can be seen from Fig. 2a that GCN-USCA performs more energy-efficient power allocation than MLP-USCA and GCN, especially in the high  $P_m$  setting. The WSEE values achieved by GCN-USCA, MLP-USCA and GCN plateau at  $P_m \approx -10$  dBW with overall averages of 6.766, 5.445, and 6.541 bit/J, respectively. On the two unfolding methods, namely GCN-USCA and MLP-USCA, the allocation performance (average WSEE values over the entire test set) is compared progressively at  $T = 7$  training milestones; see Fig. 2c. The  $t$ -th milestone is defined as the trained (partial) framework at the time point exactly before proceeding to the  $(t+1)$ -th block. Although the simple GCN does not have milestones defined, we draw a reference line at the level of its final performance. In spite of the obvious advantage of GCN-USCA over MLP-USCA which emphasizes the significance of exploiting the network topology, we also show the importance of utilizing the progressive training strategy from the following two aspects. 1) GCN-USCA reaches competitive performance with the naive GCN at the 4-th milestone, which shows that our framework, following a sophisticated unfolding architecture, can achieve higher performance with fewer parameters. 2) After the 5-th milestone, the performance of GCN-USCA cannot be further boosted by adding more blocks, which indicates that we can safely cut off at 5 blocks, further reducing the computational cost.

Finally, we discuss how prior knowledge or domain expertise can help design the learning-based framework. Recall that in proposing (12) we reasoned that the achieved WSEE should be monotonically non-decreasing with the maximum admissible power  $P_m$ . From Fig. 2a it is evident that all methods (except for the naive Max-Pow), even those learning-based, generally obey this monotonic pattern imposed by our carefully crafted regularizer. Especially, in the GCN experiment, we observed significant improvement of tuning

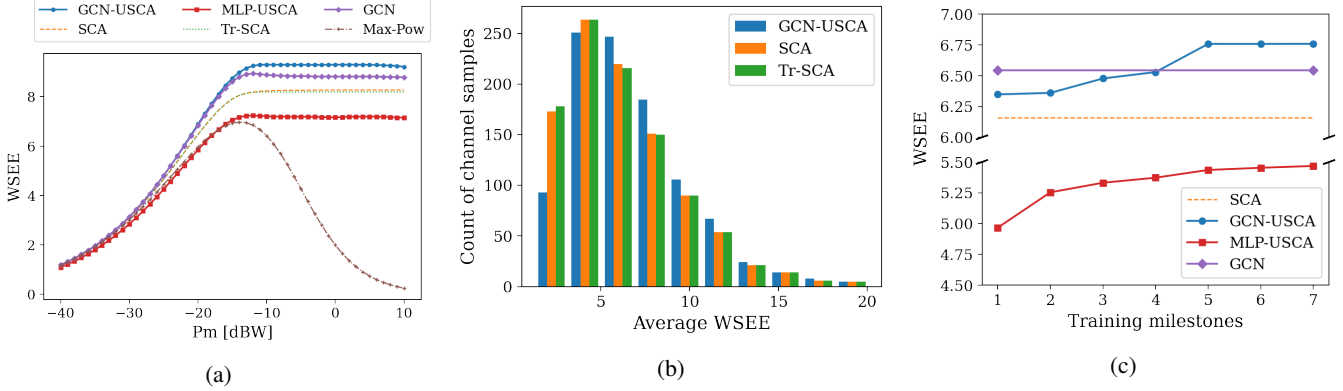


Fig. 2: Performance comparison of the proposed GCN-based USCA with SCA, a truncated version thereof, an MLP-based USCA, a GCN, and a naive policy that always allocates the maximum power  $P_m$ . (a) Performance on the test set compared with all competitor methods. Every point in the curves is given by the average WSEE over all test channel samples under the corresponding power constraint value. (b) Histogram of the achieved WSEE values for test channels compared with model-based competitor methods. Each data point represents the average WSEE value over all constraint values of a single channel sample. (c) Performance at progressive training milestones compared with learning-based competitor methods. The average WSEE values over all test channels and all constraint values are plotted against the number of unfolding blocks that have been trained and included in the framework.

TABLE I: Average WSEE values of power allocations on test sets with different number of users associated with different number of BS. The best performance for every scenario is bolded and the true optimum (when computationally feasible) is underlined.

#BS ( $M$ )	4			9			16		
#Users ( $L$ )	6	8	12	18	48	100	6	8	12
GCN-USCA	<b>5.876</b>	<b>6.766</b>	<b>8.843</b>	<b>15.518</b>	<b>31.198</b>	32.359	-	-	-
MLP-USCA	-	5.445	-	-	-	-	-	-	-
GCN	5.750	6.541	8.543	15.046	30.468	<b>33.298</b>	-	-	-
Tr-SCA	5.663	6.131	7.358	13.401	25.813	29.591	-	-	-
SCA	5.701	6.148	7.407	13.418	25.823	29.595	-	-	-
Opt	<u>6.087</u>	-	-	-	-	-	-	-	-

$\eta_m$  and eventually choose the empirical value of 0.25. This concrete example validates the importance of utilizing domain knowledge to train data-driven models for desirable behaviors.

### B. Scalability against variations in network size

Our previous results are focused on a test set with  $M = 4$  base stations and  $L = 8$  users. To demonstrate the scalability of the proposed method, we now showcase its performance with different network sizes. In particular, the scenario of varying  $L$  is of special relevance since, due to mobility, users might join and leave the system at any time. We also consider the case of varying  $M$  to assess whether a model trained on a smaller communication infrastructure can scale to a larger system. More specifically, we generate new channels with  $(L, M) \in \{(6, 4), (12, 4), (18, 9), (48, 16), (100, 16)\}$ . With these settings, we can fix either the capacity  $M$  or density  $L/M$  (average number of users served by a BS) of the network while investigating how robust our proposed method is against changes in the network size  $L$ . The models being tested are directly taken from Section IV-A (thus, trained on  $M = 4$  and  $L = 8$ ), and their performance is shown in Table I.

The first thing to notice is that, excluding the method computing the true optimum, GCN-USCA performs the best

for every configuration except for the case  $L = 100$ , where it ranks second behind GCN. Importantly, GCN-USCA beats the classical baseline SCA for every considered configuration. For the case  $M = 4$  and  $L = 6$ , the system is small enough for us to compute the true optimal power allocation. Thus, we can see that GCN-USCA reduces in 45% [(5.876 – 5.701)/(6.087 – 5.701)] the suboptimality gap of classical SCA while being computationally more efficient as illustrated in Section IV-A. Lastly, note that MLP-USCA can only be tested in the same setting on which it was trained since its input and output dimensions are fixed. This further underscores the importance of considering GCNs for the subnetworks  $\Psi$  in the unfolded architecture. GCNs not only lead to better performance within the configuration seen during training but also enable the generalization to systems of varying size, a necessary requirement in practical deployments.

### C. Robustness to path-loss model mismatches

In this section we depart from the WBS model for our PL propagation model and study how generalizable the allocation methods are to changes in the test channel distribution. The test datasets are generated following the Hata-COST231 propagation model [75]. Four types of PL effects are considered – urban or suburban environment, with or without the log-normal shadowing – with acronyms of Urb-noSF (Hata-COST231 urban model without shadowing), Sub-SF (Hata-COST231 suburban model with shadowing), Sub-noSF, and Urb-SF. We assume 1.9 GHz for the carrier frequency and 30 m for the BS height; if applicable, the standard deviation of shadowing is 8 dB. Again, for each candidate method, the model being tested here is the exact model from Section IV-A without any further processing. Numerical results are reported in Table II. Additionally, we visualize the curves of average WSEE against the power constraint  $P_m$  in the same range as before; see Fig. 3.

TABLE II: Average WSEE values of power allocations on test sets with different channel distributions as a result of different PL propagation models.

PL propagation model	Wideband spatial	Hata Urban		Hata Suburban	
		w/o SF	SF	w/o SF	SF
GCN-USCA	<b>6.766</b>	<b>7.427</b>	<b>8.501</b>	<b>10.137</b>	10.997
MLP-USCA	5.445	5.536	6.419	6.770	7.461
GCN	6.541	7.198	8.260	9.770	10.699
Tr-SCA	6.131	6.532	7.791	9.132	10.426
SCA	6.148	6.661	8.056	9.768	<b>11.298</b>
GCN-USCA <sup>+</sup>	6.771	7.548	8.676	10.737	11.699

Once more, without any retraining, GCN-USCA achieves the best performance in almost every setting only ranking second in sub-SF behind the classical SCA baseline (excluding from our analysis GCN-USCA<sup>+</sup>, which will be introduced shortly). A few observations are in order. First, the fact that GCN-USCA consistently outperforms MLP-USCA and GCN demonstrates good generalizability properties of our method compared with other learning-based approaches. Second, notice that the gap between Tr-SCA and SCA increases for the suburban channels, possibly indicating a more challenging allocation scenario. This is consistent with our (pre-trained) GCN-USCA underperforming in such a setting. Third, and more importantly, in Fig. 3 we can appreciate the root cause of the decay in average WSEE for suburban channel models. If we focus on the solid purple and red curves (and their dotted counterparts), it is clear that GCN-USCA markedly outperforms SCA even in the suburban setting for low maximum power constraints ( $P_m \leq -20$  dBW). However, for larger power constraints, GCN-USCA does not maintain the monotonicity discussed in Section III-A, thus hindering the overall average performance. Putting it differently, the monotonicity imposed via the regularizer  $\mathcal{R}_m$  in (14) does not generalize well to new channel distributions. Nonetheless, since SCA has to be sequentially solved from lower to larger values of  $P_m$  (since the solution from one value is used as a warm-start for the next one; see Footnote 1), a fairer comparison would be one where we follow the same procedure for GCN-USCA. Under such a setting, we can impose monotonicity by simply running GCN-USCA for a given  $P_m$  and, if the WSEE decreases with respect to the one obtained for a lower  $P_m$ , we simply keep the previous power allocation policy. This modified methodology gives rise to the dashed lines in Fig. 3 (illustrated for the suburban channels) and we list the obtained WSEE under GCN-USCA<sup>+</sup> in Table II. Note that for the WBS model (where training and testing follow the same channel distribution), there is neglectable difference between GCN-USCA and GCN-USCA<sup>+</sup> since monotonicity is successfully imposed (cf. Fig. 2a). On the other hand, for the suburban channels the improvement of GCN-USCA<sup>+</sup> is notable, markedly outperforming both GCN-USCA and SCA.

Overall, GCN-USCA has shown good generalizability to channel models unseen during training. However, if the mismatch between training and testing data proves to be a major problem, the learning-based method is easily improvable by transfer learning [76] given adequate (or even imperfect) data from the target distribution. This is further analyzed in the next section.

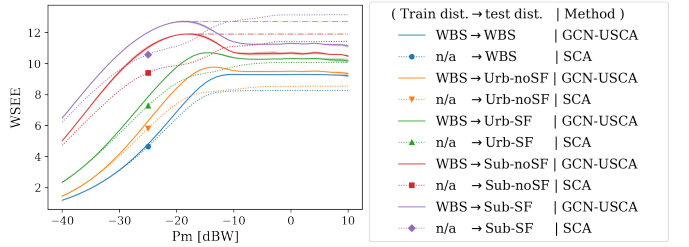


Fig. 3: Performance of GCN-USCA trained on the WBS channels and tested on different channel distributions compared with that of the classical SCA.

#### D. Impact of supervision and training set size in fine-tuning across channel distributions

We now show that, by simple fine-tuning, our proposed framework originally trained on a channel distribution can provide energy-efficient power allocation policies for a different (possibly more complicated) distribution. In particular, we focus our demonstration on transferring GCN-USCA from the WBS training channel distribution to the Sub-SF test distribution, as the previous section has indicated that this scenario is specially challenging. The fine-tuning is performed in an end-to-end manner with a universal learning rate of  $l_f = 5 \times 10^{-5}$ . Primarily, the entire set of 500 Sub-SF channels coupled with 51 constraint values are used for fine-tuning; the regularization coefficients  $\eta_m$  and  $\eta_s$  are set to be 0.25 and 0 (completely unsupervised), respectively. Within the *first* epoch, the average WSEE performance of GCN-USCA already reaches 11.445, higher than SCA's 11.298. The final average performance of GCN-USCA is 12.056, peaking at 13.289 ( $P_m = -18$  dBW) and stabilizing around 13.162 ( $P_m \geq -10$  dBW). The stationary point 13.162 is close to the peak 13.289, indicating that GCN-USCA has mostly restored monotonicity from the new distribution. As a comparable baseline, the WSEE of SCA saturates towards 13.154 as  $P_m$  approaches 10 dBW. From these observations, we find that fine-tuning across input distributions can significantly improve allocation performance and restore monotonicity on the target distribution.

Next, we proceed to study whether the utilization of imperfect “labels” can help the fine-tuning converge faster. The motivation is brought by the observation from Fig. 3 that GCN-USCA performs worse than SCA when  $P_m$  is large. Intuitively, if we train USCA to directly mimic the exact behavior of SCA under large  $P_m$  constraints, would it facilitate USCA to learn better local optima that are closer to the global solution? By examining the means of loss and regularization terms given by the base model on the training samples, we heuristically configure the loss coefficients of  $\lambda_s = 1 \times 10^3$ ,  $\eta_m = 0.25$ , and  $\eta_s = 1 \times 10^3$ . Again, all training samples are considered, but only those worse-than-SCA samples are going to be actually supervised by (inherently suboptimal) SCA labels. In that sense, we say that the supervision here is *incomplete* and *inexact*. With SCA supervision, we indeed observe faster and more stable convergence in training loss at the early stage, but not in validation; moreover, the final test

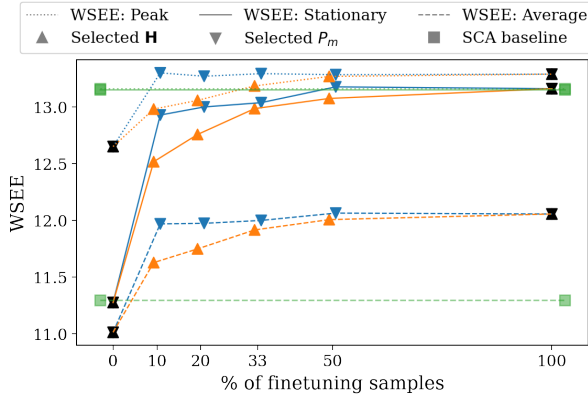


Fig. 4: Average, peak, and stationary WSEE values of finetuned GCN-USCA power allocations on test set with different amount of training samples by selecting subsets of  $P_m$  and  $\mathbf{H}$ . The SCA performance (horizontal lines) is annotated for reference.

WSEE of this supervised scheme averages at 11.990, slightly lower than the unsupervised 12.056. This indicates that the effectiveness of supervision could be limited by the quality of labels and often fail to generalize to new data, which to some extent adds on to the intuition of following an unsupervised scheme in the first place.

Finally, we investigate the minimal needed data for good unsupervised fine-tuning performance. Two sets of fine-tuned GCN-USCA performance on the Sub-SF test set are displayed in Fig. 4, resulted from selecting subsets of constraints  $P_m$  and channels  $\mathbf{H}$ , respectively. The WSEE vs  $P_m$  curves (cf. Fig. 2a) are characterized by three points – i) the average denotes the average WSEE value over all test samples; ii) the peak marks the highest achieved WSEE value within a WSEE- $P_m$  curve, which is an average value over all channel samples at a certain  $P_m$ ; iii) the stationary point represents the point toward which WSEE tends to approach as  $P_m$  grows sufficiently large, specifically defined as the mean WSEE value of all samples where  $5 < P_m \leq 10$  dBW. Ideally, the stationary point should coincide with the peak point due to monotonicity. In the GCN-USCA cases, generally speaking, fine-tuning has indeed narrowed the wide gap present in the base model, which we elaborate in the sequel.

First, it is of realistic significance to simply reduce the size of the fine-tuning set, because one would naturally favor a learning scheme that requires fewer samples and epochs. To address this need, the most straightforward implementation is to drop certain constraint values. We select subsets of  $P_m$  by increasing the sampling interval from 1 to 2,3,5, and 10 dBW, corresponding to using 100, 50, 33, 20, and 10% training samples (denoted by ‘Selected  $P_m$ ’ in Fig. 4). As indicated by the numerical results, we can achieve equally good (or even better regarding the stationary performance) performance on the new channel distribution using 50% of the training set with selected  $P_m$  values. Even with only 10% training data, finetuned GCN-USCA can easily outperform SCA and be comparable to the whole-set fine-tuning performance, especially when taking the 90% saved training time into account.

From a practical standpoint, we might lack channel samples when switching to a new environment. In this scenario, we restrict the amount of accessible  $\mathbf{H}$  samples by randomly sampling 10, 20, 33, and 50% of the entire channel set. The coupled  $P_m$  values are the complete set ranging from  $-40$  through  $10$  dBW. A strong dependency on channels is clearly revealed in Fig. 4, where the  $\mathbf{H}$ -subset performance is always lower than the  $P_m$ -subset performance with the same amount of channel-constraint samples. This indicates that diverse maximum power constraints and sufficient channel data are crucial to successful transfer learning to a new distribution.

## V. CONCLUSIONS AND FUTURE WORK

We developed USCA, a novel graph-based learning approach to allocate transmit powers with optimized EE in wireless interference networks. Using algorithm unfolding directed by classical SCA, we proposed the block-wise modular architecture of USCA that intrinsically incorporates problem-specific modules augmented by trainable components. To parameterize these components, GCNs are leveraged to make explicit use of the underlying topology of communication networks. Through extensive analyses and experiments, we have demonstrated that USCA yields solutions that are: i) Accurate, since it constantly outperforms the original algorithm and well established benchmarks; ii) Efficient, because the feedforward neural architecture, once trained, costs less time and computation than model-based methods; and iii) Distributed, owing to the decentralized implementation proposed for its modular GCN-based architecture.

A natural direction to explore next would be to obtain energy-efficient power allocation in case of higher degrees of heterogeneity, such as nonuniform system constants, user-specific power or other constraints, and different user weights. From a methodological perspective, this work also paves the way for many intriguing avenues for future research in wireless resource allocation not limited to power. First, we can dig deeper into understanding the transformed loss landscape of the sum-of-ratios fractional objective by, for example, visualizing the morphology and dynamics of loss function during training or fine-tuning. Second, in lieu of the presented post-training fine-tuning, we are interested in ways to inherently promote the model’s generalizability, e.g., alternative designs of learning components and distribution diversity in training data. Finally, a direction of practical importance is to consider scenarios where channel information is missing, noisy, or even adversarial, which may raise broader problems to address concerning network security.

## REFERENCES

- [1] S. Stanczak, M. Wiczanowski, and H. Boche, *Fundamentals of Resource Allocation in Wireless Networks: Theory and Algorithms*, vol. 3. Springer Science & Business Media, 2009.
- [2] Y. Xu, G. Gui, H. Gacanin, and F. Adachi, “A survey on resource allocation for 5G heterogeneous networks: Current research, future trends and challenges,” *IEEE Commun. Surveys & Tutorials*, 2021.
- [3] V. Chandrasekhar and J. G. Andrews, “Spectrum allocation in tiered cellular networks,” *IEEE Trans. Commun.*, vol. 57, no. 10, pp. 3059–3068, 2009.

[4] C. E. Shannon, "A mathematical theory of communication," *The Bell system technical journal*, vol. 27, no. 3, pp. 379–423, 1948.

[5] S. Chu, Y. Cui, and N. Liu, "The path towards sustainable energy," *Nature materials*, vol. 16, no. 1, pp. 16–22, 2017.

[6] I. S. M. Isa, T. E. El-Gorashi, M. O. Musa, and J. Elmirmghani, "Resilient energy efficient healthcare monitoring infrastructure with server and network protection," *arXiv preprint arXiv:2010.15683*, 2020.

[7] C. Zhang, X. Wang, A. Dong, Y. Zhao, Q. He, and M. Huang, "Energy efficient network service deployment across multiple SDN domains," *Computer Commun.*, vol. 151, pp. 449–462, 2020.

[8] G. Manogaran and B. S. Rawal, "An efficient resource allocation scheme with optimal node placement in iot-fog-cloud architecture," *IEEE Sensors Journal*, 2021.

[9] C. F. Calvillo, A. Sánchez-Miralles, and J. Villar, "Energy management and planning in smart cities," *Renewable and Sustainable Energy Reviews*, vol. 55, pp. 273–287, 2016.

[10] Q. Yu, Y. Zhao, L. Zhang, K. Yang, and S. Leng, "A fair resource allocation algorithm for data and energy integrated communication networks," *Mobile Inf. Syst.*, vol. 2016, 2016.

[11] Z.-Q. Luo and W. Yu, "An introduction to convex optimization for communications and signal processing," *IEEE J. Sel. Areas Commun.*, vol. 24, no. 8, pp. 1426–1438, 2006.

[12] J. Mattingley and S. Boyd, "Real-time convex optimization in signal processing," *IEEE Signal Process. Mag.*, vol. 27, no. 3, pp. 50–61, 2010.

[13] A. B. Gershman, N. D. Sidiropoulos, S. Shahbazpanahi, M. Bengtsson, and B. Ottersten, "Convex optimization-based beamforming," *IEEE Signal Process. Mag.*, vol. 27, no. 3, pp. 62–75, 2010.

[14] Z.-Q. Luo and S. Zhang, "Dynamic spectrum management: Complexity and duality," *IEEE J. Sel. Topics Signal Process.*, vol. 2, no. 1, pp. 57–73, 2008.

[15] Y. Li, M. Sheng, C. Yang, and X. Wang, "Energy efficiency and spectral efficiency tradeoff in interference-limited wireless networks," *IEEE Commun. Lett.*, vol. 17, no. 10, pp. 1924–1927, 2013.

[16] L. Salaün, C. S. Chen, and M. Coupechoux, "Optimal joint subcarrier and power allocation in NOMA is strongly NP-hard," in *IEEE Intnl Conf. on Commun.*, pp. 1–7, IEEE, 2018.

[17] B. Matthiesen, Y. Yang, and E. A. Jorswieck, "Optimization of weighted individual energy efficiencies in interference networks," in *IEEE Wireless Commun. and Netw. Conf.*, pp. 1–6, IEEE, 2018.

[18] B. Matthiesen, A. Zappone, K.-L. Besser, E. A. Jorswieck, and M. Debbah, "A globally optimal energy-efficient power control framework and its efficient implementation in wireless interference networks," *IEEE Trans. Signal Process.*, vol. 68, pp. 3887–3902, 2020.

[19] J. Jin and A. Wang, "Multiple-objective power control algorithm based on successive interference cancellation algorithm," in *IEEE Intnl Conf. on Software Eng. and Service Sc.*, pp. 278–283, IEEE, 2020.

[20] F. Fang, H. Zhang, J. Cheng, and V. C. Leung, "Energy-efficient resource allocation for downlink non-orthogonal multiple access network," *IEEE Trans. Commun.*, vol. 64, no. 9, pp. 3722–3732, 2016.

[21] Z. Zhou, K. Ota, M. Dong, and C. Xu, "Energy-efficient matching for resource allocation in D2D enabled cellular networks," *IEEE Trans. Vehicular Tech.*, vol. 66, no. 6, pp. 5256–5268, 2016.

[22] L. Dong and G. Ren, "Optimal and low complexity algorithm for energy efficient power allocation with sensing errors in cognitive radio networks," in *Intl. Conf. on Wireless Commun. and Sig. Process.*, pp. 1–5, IEEE, 2014.

[23] F. Fang, Z. Ding, W. Liang, and H. Zhang, "Optimal energy efficient power allocation with user fairness for uplink MC-NOMA systems," *IEEE Wireless Commun. Lett.*, vol. 8, no. 4, pp. 1133–1136, 2019.

[24] H. M. Al-Obiedollah, K. Cumanan, J. Thiyyagalingam, A. G. Burr, Z. Ding, and O. A. Dobre, "Energy efficient beamforming design for MISO non-orthogonal multiple access systems," *IEEE Trans. Commun.*, vol. 67, no. 6, pp. 4117–4131, 2019.

[25] K. Long, W. Li, M. Jiang, and J. Lu, "Non-cooperative game-based power allocation for energy-efficient NOMA heterogeneous network," *IEEE Access*, vol. 8, pp. 49596–49609, 2020.

[26] Y. Yang and M. Pesavento, "A unified successive pseudoconvex approximation framework," *IEEE Trans. Signal Process.*, vol. 65, no. 13, pp. 3313–3328, 2017.

[27] B. Su, Z. Qin, and Q. Ni, "Energy efficient uplink transmissions in LoRa networks," *IEEE Trans. Commun.*, vol. 68, no. 8, pp. 4960–4972, 2020.

[28] C. N. Efrem and A. D. Panagopoulos, "Dynamic energy-efficient power allocation in multibeam satellite systems," *IEEE Wireless Commun. Lett.*, vol. 9, no. 2, pp. 228–231, 2019.

[29] Y. Li, M. Sheng, X. Wang, Y. Zhang, and J. Wen, "Max-min energy-efficient power allocation in interference-limited wireless networks," *IEEE Trans. Vehicular Tech.*, vol. 64, no. 9, pp. 4321–4326, 2014.

[30] A. Zappone, E. Björnson, L. Sanguinetti, and E. Jorswieck, "Globally optimal energy-efficient power control and receiver design in wireless networks," *IEEE Trans. Signal Process.*, vol. 65, no. 11, pp. 2844–2859, 2017.

[31] S. S. Vilni, "Energy efficient distributed worst case robust power allocation in massive MIMO," *arXiv preprint arXiv:1804.04267*, 2018.

[32] N. Rajapaksha, K. Manosha, N. Rajatheva, and M. Latva-aho, "Deep learning-based power control for cell-free massive MIMO networks," *arXiv preprint arXiv:2102.10366*, 2021.

[33] H. Lee, H. S. Jang, and B. C. Jung, "Improving energy efficiency fairness of wireless networks: A deep learning approach," *Energies*, vol. 12, no. 22, p. 4300, 2019.

[34] H. Sun, X. Chen, Q. Shi, M. Hong, X. Fu, and N. D. Sidiropoulos, "Learning to optimize: Training deep neural networks for interference management," *IEEE Trans. Signal Process.*, vol. 66, no. 20, pp. 5438–5453, 2018.

[35] D. Xu, X. Chen, C. Wu, S. Zhang, S. Xu, and S. Cao, "Energy-efficient subchannel and power allocation for HetNets based on convolutional neural network," in *IEEE Vehicular Tech. Conf.*, pp. 1–5, IEEE, 2019.

[36] W. Lee, M. Kim, and D.-H. Cho, "Deep power control: Transmit power control scheme based on convolutional neural network," *IEEE Commun. Lett.*, vol. 22, no. 6, pp. 1276–1279, 2018.

[37] Y. Zhao, I. Niemegeers, and S. H. de Groot, "Power allocation in mmwave cell-free massive MIMO with user mobility using deep learning," in *IEEE Int'l. Conf. on Commun. Tech.*, pp. 264–269, IEEE, 2020.

[38] M. Eisen, C. Zhang, L. F. Chamom, D. D. Lee, and A. Ribeiro, "Learning optimal resource allocations in wireless systems," *IEEE Trans. Signal Process.*, vol. 67, no. 10, pp. 2775–2790, 2019.

[39] Y. S. Nasir and D. Guo, "Multi-agent deep reinforcement learning for dynamic power allocation in wireless networks," *IEEE J. Sel. Areas Commun.*, vol. 37, no. 10, pp. 2239–2250, 2019.

[40] M. Eisen and A. Ribeiro, "Optimal wireless resource allocation with random edge graph neural networks," *IEEE Trans. Signal Process.*, vol. 68, pp. 2977–2991, 2020.

[41] H. Sun, X. Chen, Q. Shi, M. Hong, X. Fu, and N. D. Sidiropoulos, "Learning to optimize: Training deep neural networks for wireless resource management," in *IEEE Int'l. Wrksp. on Sig. Process. Advances in Wireless Commun.*, pp. 1–6, IEEE, 2017.

[42] T. Van Chien, T. Nguyen Canh, E. Björnson, and E. G. Larsson, "Power control in cellular massive MIMO with varying user activity: A deep learning solution," *IEEE Trans. Wireless Commun.*, vol. 19, no. 9, pp. 5732–5748, 2020.

[43] A. Chowdhury, G. Verma, C. Rao, A. Swami, and S. Segarra, "Unfolding WMMSE using graph neural networks for efficient power allocation," *IEEE Transactions on Wireless Communications*, 2021.

[44] C.-H. Lin, Y.-T. Lee, W.-H. Chung, S.-C. Lin, and T.-S. Lee, "Unsupervised ResNet-inspired beamforming design using deep unfolding technique," in *GLOBECOM 2020-2020 IEEE Global Communications Conference*, pp. 1–7, IEEE, 2020.

[45] L. Pellaco, M. Bengtsson, and J. Jaldén, "Deep unfolding of the weighted MMSE beamforming algorithm," *arXiv preprint arXiv:2006.08448*, 2020.

[46] A. Kumar, G. Verma, C. Rao, A. Swami, and S. Segarra, "Adaptive contention window design using deep Q-learning," in *IEEE Int. Conf. on Acoustics, Speech and Signal Process.*, pp. 4950–4954, 2021.

[47] Z. Zhao, G. Verma, C. Rao, A. Swami, and S. Segarra, "Distributed scheduling using graph neural networks," in *IEEE Int. Conf. on Acoustics, Speech and Signal Process.*, pp. 4720–4724, 2021.

[48] B. C. Csáji *et al.*, "Approximation with artificial neural networks," *Faculty of Sciences, Eötvös Loránd University, Hungary*, vol. 24, no. 48, p. 7, 2001.

[49] V. Monga, Y. Li, and Y. C. Eldar, "Algorithm unrolling: Interpretable, efficient deep learning for signal and image processing," *arXiv preprint arXiv:1912.10557*, 2019.

[50] A. Chowdhury, G. Verma, C. Rao, A. Swami, and S. Segarra, "Efficient power allocation using graph neural networks and deep algorithm unfolding," in *IEEE Int. Conf. on Acoustics, Speech and Signal Process.*, pp. 4725–4729, 2021.

[51] K. Gregor and Y. LeCun, "Learning fast approximations of sparse coding," in *Intl. Conf. on Machine Learning*, pp. 399–406, 2010.

[52] K. Zhang, L. V. Gool, and R. Timofte, "Deep unfolding network for image super-resolution," in *Proceedings of the IEEE/CVF Conf. on Computer Vision and Pattern Recognition*, pp. 3217–3226, 2020.

[53] S. Wisdom, J. Hershey, J. Le Roux, and S. Watanabe, "Deep unfolding for multichannel source separation," in *IEEE Int. Conf. on Acoustics, Speech and Signal Process.*, pp. 121–125, IEEE, 2016.

- [54] Z. Zhang, Y. Liu, J. Liu, F. Wen, and C. Zhu, “AMP-Net: Denoising-based deep unfolding for compressive image sensing,” *IEEE Trans. on Img. Process.*, vol. 30, pp. 1487–1500, 2020.
- [55] S. Chen, Y. C. Eldar, and L. Zhao, “Graph unrolling networks: Interpretable neural networks for graph signal denoising,” *arXiv preprint arXiv:2006.01301*, 2020.
- [56] Q. Hu, Y. Cai, Q. Shi, K. Xu, G. Yu, and Z. Ding, “Iterative algorithm induced deep-unfolding neural networks: Precoding design for multiuser MIMO systems,” *IEEE Trans. Wireless Commun.*, 2020.
- [57] R. W. Freund and F. Jarre, “Solving the sum-of-ratios problem by an interior-point method,” *J. of Global Optim.*, vol. 19, no. 1, pp. 83–102, 2001.
- [58] A. Zappone, M. Di Renzo, and M. Debbah, “Wireless networks design in the era of deep learning: Model-based, AI-based, or both?,” *IEEE Trans. Commun.*, vol. 67, no. 10, pp. 7331–7376, 2019.
- [59] A. Balatsoukas-Stimming and C. Studer, “Deep unfolding for communications systems: A survey and some new directions,” in *IEEE Intl. Wrksp. Signal Process. Sys. (SIPS)*, pp. 266–271, IEEE, 2019.
- [60] J. R. Hershey, J. L. Roux, and F. Weninger, “Deep unfolding: Model-based inspiration of novel deep architectures,” *arXiv preprint arXiv:1409.2574*, 2014.
- [61] T. N. Kipf and M. Welling, “Semi-supervised classification with graph convolutional networks,” *IEEE Intnl Conf. on Learning Repr.*, 2017.
- [62] F. Gama, A. G. Marques, G. Leus, and A. Ribeiro, “Convolutional neural network architectures for signals supported on graphs,” *IEEE Trans. Signal Process.*, vol. 67, no. 4, pp. 1034–1049, 2018.
- [63] T. M. Roddenberry and S. Segarra, “Hodgenet: Graph neural networks for edge data,” in *Asilomar Conf. on Sig., Sys., and Computers*, pp. 220–224, IEEE, 2019.
- [64] L. Armijo, “Minimization of functions having Lipschitz continuous first partial derivatives,” *Pacific Journal of mathematics*, vol. 16, no. 1, pp. 1–3, 1966.
- [65] A. Ben-Tal and A. Nemirovski, “Robust convex optimization,” *Mathematics of operations research*, vol. 23, no. 4, pp. 769–805, 1998.
- [66] S. Bubeck, “Convex optimization: Algorithms and complexity,” *arXiv preprint arXiv:1405.4980*, 2014.
- [67] P. J. Huber, “Robust estimation of a location parameter,” in *Breakthroughs in statistics*, pp. 492–518, Springer, 1992.
- [68] K. Wu, Y. Guo, Z. Li, and C. Zhang, “Sparse coding with gated learned ISTA,” in *IEEE Intnl Conf. on Learning Repr.*, 2019.
- [69] X. Chen, J. Liu, Z. Wang, and W. Yin, “Theoretical linear convergence of unfolded ISTA and its practical weights and thresholds,” in *Intl. Conf. on Neural Inf. Process. Sys.*, pp. 9079–9089, 2018.
- [70] M. D. Zeiler and R. Fergus, “Visualizing and understanding convolutional networks,” in *European Conf. on Comp. Vision*, pp. 818–833, Springer, 2014.
- [71] S. Segarra, A. G. Marques, and A. Ribeiro, “Optimal graph-filter design and applications to distributed linear network operators,” *IEEE Trans. Signal Process.*, vol. 65, no. 15, pp. 4117–4131, 2017.
- [72] F. Gama, J. Bruna, and A. Ribeiro, “Stability properties of graph neural networks,” *IEEE Trans. Signal Process.*, vol. 68, pp. 5680–5695, 2020.
- [73] G. Calcev, D. Chizhik, B. Goransson, S. Howard, H. Huang, A. Kogiantis, A. F. Molisch, A. L. Moustakas, D. Reed, and H. Xu, “A wideband spatial channel model for system-wide simulations,” *IEEE Trans. Vehicular Tech.*, vol. 56, no. 2, pp. 389–403, 2007.
- [74] M. D. Zeiler, “Adadelta: an adaptive learning rate method,” *arXiv preprint arXiv:1212.5701*, 2012.
- [75] E. Damosso, L. M. Correia, *et al.*, “Digital mobile radio towards future generation systems,” *COST 231 final report*, p. 474, 1999.
- [76] R. Dong, C. She, W. Hardjawana, Y. Li, and B. Vucetic, “Deep learning for radio resource allocation with diverse quality-of-service requirements in 5G,” *IEEE Trans. Commun.*, 2020.